Photochemistry and Photobiology, 2006, 82: 1279–1284

Research Note

Real-time *In Situ* Monitoring of Human Prostate Photodynamic Therapy with Diffuse Light

Guoqiang Yu[1]*, Turgut Durduran[1], Chao Zhou[1], Timothy C. Zhu[2], Jarod C. Finlay[2], Theresa M. Busch[2], S. Bruce Malkowicz[3], Stephen M. Hahn[2] and Arjun G. Yodh[1]

[1]Department of Physics & Astronomy, University of Pennsylvania, Philadelphia, PA
[2]Department of Radiation Oncology, University of Pennsylvania, Philadelphia, PA
[3]Department of Urology, University of Pennsylvania, Philadelphia, PA

Received 19 October 2005; accepted 10 May 2006; published online 12 May 2006 DOI: 10.1562/2005-10-19-RA-721

ABSTRACT

Photodynamic therapy (PDT) requires oxygen to cause cellular and vascular tumor damage. Tissue oxygen concentration, in turn, is influenced by blood flow and blood oxygenation. Real-time clinical measurement of these hemodynamic quantities, however, is rare. This paper reports the development and application of a probe, combining diffuse reflectance spectroscopy (DRS) for measurement of tumor blood oxygenation and diffuse correlation spectroscopy (DCS) for measurement of tumor blood flow. The instrument was adapted for clinical use *during* interstitial prostate PDT. Three patients with locally recurrent prostate cancer received 2 mg/kg motexafin lutetium (MLu) 3 h before illumination and a total light dose of 100 J/cm^2 at 150 mW/cm. Prostrate blood oxygen saturation (StO_2) decreased only slightly (~3%) after treatment. On the other hand, prostate blood flow and total hemoglobin concentration over the course of PDT decreased by 50% and 15%, respectively, suggesting MLu-mediated PDT has an anti-vascular effect. While it is certainly impossible to draw definite conclusions from measurements of only three patients, the observed differences in tumor blood flow and blood oxygenation responses during PDT can, in principle, be used to choose among tissue oxygen consumption models and therefore emphasize the potential clinical value for simultaneous monitoring of both parameters.

INTRODUCTION

Photodynamic therapy (PDT) (1,2) is an evolving cancer treatment that uses light to activate a photosensitizing drug. In the presence of tissue oxygen, activated photosensitizer initiates a cascade of chemical reactions producing necrosis and apoptosis of tumor cells and vascular damage. Tissue oxygen concentration, in turn, is influenced by blood flow and blood oxygenation. Several techniques have been applied for measuring tissue oxygenation and blood flow. Polarographic electrodes and O_2 microelectrodes facilitate invasive measurements of tissue partial oxygen pressure (pO_2) (3–6). However, the invasive nature and poor spatial resolution of both techniques limits their application. BOLD-contrast magnetic resonance imaging (MRI) has been applied in PDT for monitoring hemoglobin saturation levels in animal models (7). However, its clinical use in a procedure like PDT is limited by high cost and poor mobility. Laser Doppler (8,9) and optical coherence tomography (OCT) (10,11) can non-invasively monitor blood flow, but most of these systems measure only the tissue surface (penetration depth < 1 mm). Power Doppler ultrasound can non-invasively follow tumor perfusion after PDT (12), but does not readily permit continuous measurement during PDT.

Near-infrared spectroscopy (NIRS) permits noninvasive measurements of total hemoglobin concentration and blood oxygen saturation at distances of up to several centimeters below the tissue surface (13–15). Similarly, near-infrared diffuse correlation spectroscopy (DCS) is an emerging technique for measurement of microvascular blood flow within deep tissues (16). We have developed a multi-modality near-infrared diffuse optical instrument combining diffuse reflectance spectroscopy (DRS) for measurement of tissue blood oxygenation, with DCS for measurement of tissue blood flow. This instrumentation is portable, inexpensive, and fast. It has been used to study tissue response in a variety of physiological contexts, for example functional imaging and spectroscopy of brain (17–20), tumor physiology (21,22), photodynamic therapy in animals (23), and exercising muscles (24). Measurements of blood flow by DCS have been validated against color power Doppler Ultrasound in tumors (23) and laser Doppler in brain (17,18). DRS for tissue blood oxygenation measurement has also been validated in phantoms and different tissues *in vivo* (25–28). Presently it is difficult to carry out concurrent measurements with other technologies in such a small target volume (prostate) without influencing the interstitial PDT treatment.

In this study, we explore the feasibility for adapting this diffuse optical instrument to monitor tissue blood flow and oxygenation continuously during interstitial prostate PDT. Prostate adenocarcinoma is the most common malignancy in men (29). A Phase I trial of interstitial PDT is underway at the University of Pennsylvania,

*Corresponding author email: guoqiang@physics.upenn.edu (Guoqiang Yu)

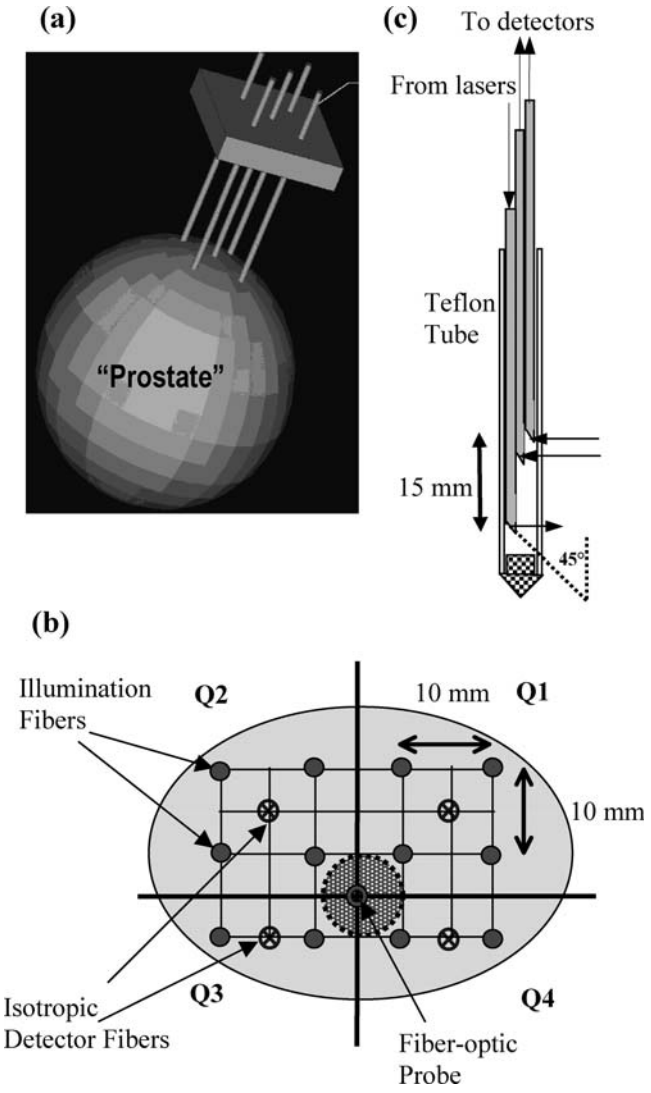

Figure 1. Custom-made template for one quadrant (Fig. 1a) and cross-sectional view (Fig. 1b) of the fiber positions for all quadrants in the gland of a typical patient. The 732 nm treatment light was administered through the cylindrical diffusing fibers inside the catheters (solid-circles). The distribution of the treatment light during the PDT was monitored by an isotropic-detector fiber (cross-circles) placed in the center of source fibers (cross-circles). Four quadrants of the prostate (Q1 to Q4) were illuminated sequentially in sessions until the entire gland was treated. Our fiber-optic probe was placed before treatment through the catheter in the center of the quadrants (double-circle) and stayed in place throughout PDT. The darkly shaded area demonstrates approximately the bulk tissue area monitored continuously by the fiber-optic probe. The fiber-optic probe (Fig. 1c) for the use of interstitial prostate PDT had one source and five detector fibers (only one source fiber and two detector fibers are shown for clarity). The source-detector separations range from 0.5 to 1.5 cm. In order to couple the light out of the fiber into the tissues and vice versa, the fiber tip was cut and polished to form a 45° with the fiber central axis. Total internal reflection occurs at this boundary, and more than 80% power of incident light can be delivered to the tissue.

using the photosensitizer motexafin lutetium (MLu) (30,31) in men with locally recurrent prostate cancer (32,33). To adapt the optical system for use in this clinical trial, a fiber-optic probe containing source and detector fibers was constructed. This probe was placed inside an 18-gauge catheter that had already been inserted into the patient's prostate gland. Using this probe, we successfully monitored tumor hemodynamic responses during interstitial PDT. To our knowledge this class of clinical measurement during interstitial PDT has not previously been reported.

MATERIALS AND METHODS

Protocol. The clinical study was approved by the Institutional Review Board (IRB) at the University of Pennsylvania. Each patient signed the informed consent document. Motexafin lutetium (MLu, Pharmacyclics, Inc., Sunnyvale, CA) was administered at a dose of 2 mg/kg intravenously 3 h prior to light administration (31–33). The patients were anesthetized in the operating room and an endorectal ultrasound probe was introduced. A standard brachytherapy transperineal implant template was attached to the ultrasound unit, and plastic brachytherapy 18-gauge catheters (Flexineedle, Best Medical International Inc., VA) were guided into the prostate through the perineal template. The cylindrical diffusing fibers (line sources) were then introduced through the catheters (solid-circles in Fig. 1b), and 732 nm light was administered at an intensity of 150 mW/cm (*i.e*. 150 mW is emitted cylindrically from each cm of source fiber). The patients received a total light dose (fluence) of 100 J/cm^2. The light distribution and total light dose were monitored by the isotropic-detector fibers (cross-circles in Fig. 1b). Interstitial PDT was designed to comprehensively treat the entire prostate gland. Depending on the gland volume of each individual, illuminations from three or four quadrants of the prostate were carried out sequentially until the entire gland was treated with the correct dose. Light emitted into one quadrant often propagated to nearby quadrants. Figure 1 shows an implant template for one quadrant (Fig. 1a) and cross-sectional view of the fiber positions for all quadrants in the gland (Fig. 1b). Our fiber-optic probe was placed through the 18-gauge catheter in the center of the gland (double-circle in Fig. 1b) before treatment; it remained in place throughout PDT treatment. Tissue hemodynamics were continuously monitored for several minutes between quadrant illuminations. Immediately after the treatment, the fiber-optic probe was withdrawn from the prostate and placed within another catheter, which subsequently was immersed in several liquid phantoms (Intralipid +~~←~~India ink) with known optical properties for calibration measurements.

Novel fiber-optic probe. Our previous instruments were poorly suited for interstitial measurements such as prostate PDT. In order to use the existing PDT treatment catheters and minimize treatment perturbations, a thin transparent fiber-bundled probe was developed. The probe could be readily placed into an 18-gauge catheter. One source and five detector fibers were bundled inside a transparent Teflon tube (FiberOptics, Inc., CA) with diameter less than 1 mm. Only three fibers are shown in Fig. 1c for clarity. The source fiber (shared by both DRS and DCS) was multimode with diameter d = 200 μm. Three multimode fibers (d = 100 μm) were used to detect light for DRS measurements. Two single-mode fibers (d = 7 μm) were employed for DCS measurements. In order to couple light into the tissue and vice versa, the fiber tip was cut and polished to form a 45° with the fiber central axis. Incident light experienced total internal reflection at the fiber-air boundary and entered the tissue at right angles to the fiber central axis. More than 80% of the incident light was delivered into the tissue using this side-illuminating fiber. The source and detector fibers protruded different depths into the tissue, enabling simultaneous measurement in different locations. Detector fibers for DRS were located 5, 10, and 15 mm away from the source fiber; separations for DCS were 10 and 15 mm. From simulation results using three-point Green's functions in infinite media, we find that the maximum light penetration depth for the separation of 10–15 mm is approximately 4–5 mm (this estimate is for paths wherein the probability that a photon leaves the source, arrives at the detector and passes through selected tissue volume is greater than 50%). For simplicity, the simulated tissue was assumed homogeneous (μ_a = 0.2 cm ^{1}; μ_s' = 13 cm ^{1}), and the influence of the thin fiber-optic probe on light transport was neglected. The cross-sectional view of the maximum sample area is shown as a darkly shaded area in Fig. 1b.

Hybrid diffuse optical instrument. Details of this instrument are described elsewhere (17,18,24). Briefly, light from amplitude-modulated (70 MHz) lasers operating at 690, 785, and 830 nm were fiber-coupled onto the tissue surface. Photons transmitted into the tissue were detected in reflection. These wavelength-dependent data were used to determine the oxyhemoglobin and deoxyhemoglobin concentrations by near-infrared (NIR) spectroscopic analysis. A narrowband cw laser (800 nm), four photon-counting, fast avalanche photodiodes, and a four-channel autocorrelator

board facilitated measurements of blood flow; temporal autocorrelation functions of the reflected light were used to derive flow information (34).

DRS for tissue blood oxygenation. Prostate tissue was approximated as an infinite homogeneous medium, and an infinite analytical solution to the photon diffusion equation for this geometry was used to fit for the bulk tissue properties (absorption coefficient, μ_a, and reduced scattering coefficient, μ_s') (34). The analysis minimized $\chi^2 = \sum \|\Phi_m(t)/\Phi_{m\_ref} \Phi_c(t)/\Phi_{c\_ref}\|^2$. Here $\Phi_m(t)$ and $\Phi_c(t)$ are the measured and calculated light fluence rates at time (t), respectively. Φ_{m_ref} and Φ_{c_ref} are the measured and calculated light fluence rates from our calibration phantom with known optical properties. The sum is over the large-separation source-detector pairs (*i.e*. 10 mm and 15 mm). This choice of source-detector separation insured the same tissues were sampled as in the DCS measurements. This method worked well for amplitude signals in phantoms and *in vivo* tissues, but the phase signals were noisier than amplitude signals; we therefore dropped phase from our analysis. This analysis, therefore, required some independent knowledge about the reduced scattering coefficient. Our model assumed a baseline reduced scattering coefficient, $\mu_s' = 13\ cm^{-1}$ (32). The wavelength-dependent μ_a was then decomposed into oxy-hemoglobin concentration (C_{HbO_2}) and deoxy-hemoglobin concentration (C_{Hb}) (24). Combinations of these parameters yielded total hemoglobin concentration ($THC = C_{Hb} + C_{HbO_2}$) and blood oxygen saturation ($StO_2 = [C_{HbO_2}/(C_{Hb} + C_{HbO_2})] \times 100$).

DCS for relative blood flow. Speckle fluctuations of the diffuse light (35,36) are sensitive to the motions of tissue scatterers such as red blood cells. The quantity containing this information is the electric field (E(r, t)). The electric field temporal autocorrelation function, $G_1(r, \tau) = \langle E(r, t)E^*(r, t + \tau)\rangle$, or its Fourier Transform is explicitly related to the motion of the scatterers (*e.g*., red blood cells). Here the angle brackets $\langle\ \rangle$ denote averages over time and τ is called the correlation delay time. From the (normalized) intensity autocorrelation function measured by DCS, we calculate the normalized electric field temporal autocorrelation function $g_1(r, \tau) = G_1(r, \tau)/\langle E(r, t)\, E^*(r, t)\rangle$; $G_1(r, \tau)$ satisfies the correlation diffusion equation in highly scattering media (16,37). The exact form of the correlation diffusion equation depends on the nature and heterogeneity of the particle motion. For the case of diffusive motion, $\langle \Delta r^2(\tau)\rangle = 6D_B\tau$, where D_B is an effective diffusion coefficient of the moving scatterers (18,34). In this case the normalized correlation function $g_1(r, \tau)$ will decay at early time approximately exponentially in τ. Its decay depends on a parameter α (proportional to the tissue blood volume fraction), and on the mean-square displacement of the blood cells. Relative changes of αD_B are correlated with relative changes in tissue blood flow (16–19,22). The bulk flow responses derived in this paper utilized averaged data from source-detector separations of 10 and 15 mm.

In the calculation of blood oxygenation and flow, it is possible that uncertainty of the assumed baseline value of the scattering coefficient μ_s' may introduce systematic effects (38). These potential sources of error were investigated by varying the assumed value of μ_s' and then computing the relative changes of oxygenation and flow. We found empirically that a 100% change in baseline μ_s' introduced less than a 5% error in the calculated *relative* change of total hemoglobin concentration (rTHC) and oxygen saturation ($rStO_2$). The error induced in the calculated rBF was less than 1%. On the other hand, if μ_s' changed *during* treatment then the effect on rBF, rTHC and $rStO_2$ would be larger (*i.e*. ~15% in rBF, ~5% in rTHC, and ~1% in $rStO_2$ for 25% change in μ_s' during treatment).

Suppression of treatment light. PDT treatment excitation light at 732 nm can interfere with our optical measurements. In order to monitor hemodynamic changes during illumination, two sets of optical filters were placed in front of the detectors to attenuate this excitation light: a narrow-band notch filter (732 ± 5 nm, Kaiser Optical Systems, Inc., Michigan) for DRS, and a narrow-band pass filter (800 ± 10 nm, Chroma Technology, Corp., VT) for DCS. The light transmission through the filters was less than 0.01% at 732 nm, and was more than 80% at our probe wavelengths. The filters were tested by comparing the detected signals with/without treatment light (732 nm) in a tissue phantom. Potential interference was below our experimental noise level.

Instrumentation evaluation in liquid tissue phantoms. The fiber-optic probe was tested in the liquid phantoms. The liquid phantoms were composed of Intralipid and India Ink. They were prepared according to an old recipe (27,34). The absorption properties (μ_a) were estimated for each preparation (prior to the inclusion of scatterers) using a spectrophotometer (27). We have measured the repeatability of this process and found the error to be less than 5%. The scattering properties (μ_s') had errors of ~10%. Inaccuracies of the phantom preparation had an even smaller effect on calibrations and did not substantially perturb the relative change measurements (27).

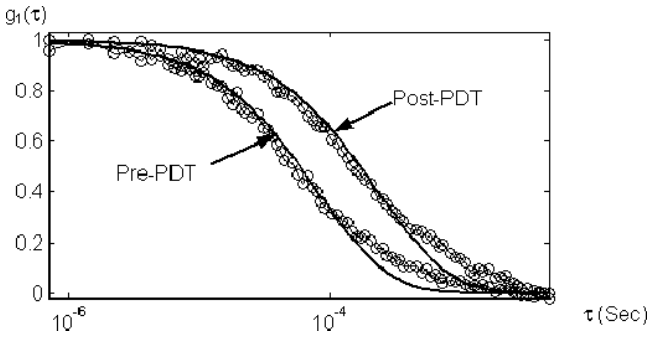

Figure 2. Typical normalized electric field autocorrelation function $g_1(\tau)$ (circles) in a prostate patient before and after PDT. The source-detector separation was 10 mm. Fits (solid line) using the Brownian diffusion model are also shown. The post-PDT autocorrelation curve decays slower than that of pre-PDT, indicating reduction in blood flow after PDT treatment.

The catheter containing the fiber-optic probe was immersed in the liquid phantoms to simulate the clinical measurement configuration (shown in Fig. 1b). Using this configuration we carried out the following tests: (1) Measurement repeatability, *i.e*. characterized by the coefficient of variation (CV) of multiple measurements (n = 5). Amplitude signals for DRS and relative changes in αD_B for DCS were evaluated. (2) Influence of treatment light, *i.e*. the difference of measured signals with and without treatment illumination. (3) Disturbance of the treatment light distribution, *i.e*. the difference of treatment light distribution with and without the fiber-optic probe. (4) Measurement accuracy of the absorption coefficient, μ_a. Five tissue phantoms were used for these studies. The reduced scattering coefficient of these tissue phantoms was fixed at $\mu_s' = 13\ cm^{-1}$, and the absorption coefficient μ_a was 0.1, 0.15, 0.2, 0.25 or 0.3 cm^{-1} at 786 nm. The sample with median value ($\mu_a = 0.2\ cm^{-1}$) was used as a 'standard' sample by which to calibrate all other samples.

RESULTS

Tissue phantom test

The coefficient of variation of multiple measurements (n = 5) with multiple separations (5 to 15 mm) was less than 3% and 5% for diffuse reflectance spectroscopy (DRS) and diffuse correlation spectroscopy (DCS), respectively. The variation with and without illumination fell within this range, indicating that the optical filters effectively attenuated the excitation light. The fiber-optic probe caused only minor (<4%) perturbation of the treatment light distribution. Five tissue phantoms ($\mu_a = 0.1$ to 0.3 cm^{-1} @ 786 nm) were used for evaluation of the measurement accuracy. The μ_a errors were less than 10%. The *absolute* value of the oxygen saturation has an error similar in order to the error of the individual absorption coefficients. However, the *relative* changes of oxygen saturation are less sensitive than the absolute changes (13,26,27). We have estimated this error in the *relative* change to be <3%.

Pre- and post-PDT autocorrelation functions

We successfully measured 3 patients with locally recurrent prostate cancer. Figure 2 shows typical DCS measurements of the normalized electric field temporal autocorrelation function $g_1(\tau)$ from one prostate patient before and after PDT. Data points (circles) are fit using the Brownian diffusion model (17,18). The post-PDT autocorrelation curve decays much slower than that of pre-PDT, indicating a decrease in blood flow after PDT.

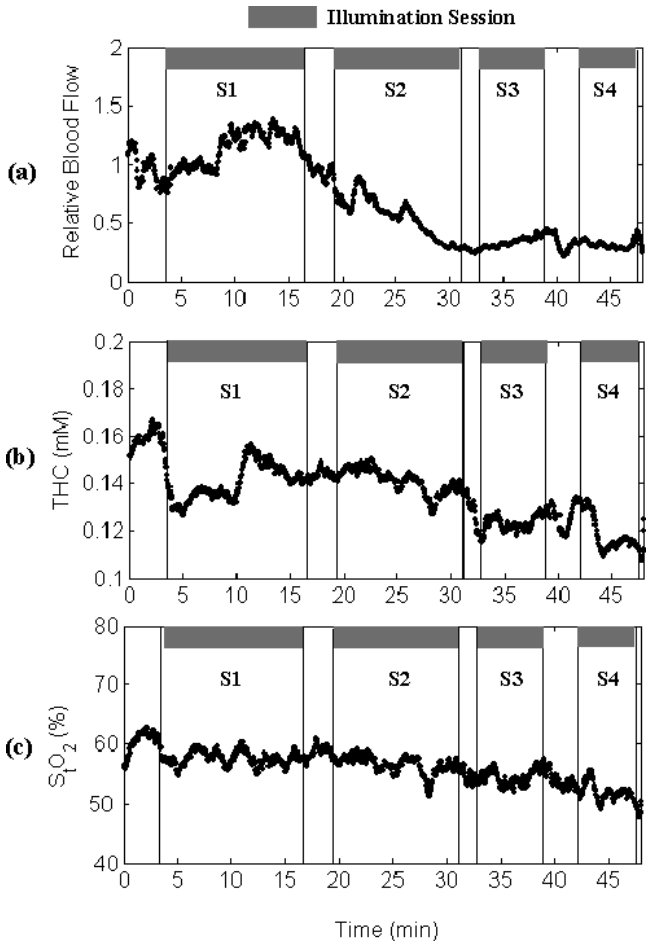

Figure 3. Time course of prostate hemodynamic properties. Individual panels from top to bottom demonstrate, respectively, the dynamic changes in relative blood flow (Fig. 3a), total hemoglobin concentration (Fig. 3b), and tissue blood oxygen saturation (Fig. 3c). The prostate was illuminated sequentially in four sessions (S1 to S4) until the entire gland was treated. The illumination periods correspond are presented as shaded bars.

Hemodynamic responses in prostate patients

Figure 3 shows the typical time course of hemodynamic changes during prostate PDT in a patient. In each patient the prostate quadrants were treated sequentially in individual illumination sessions (S1 to S4). Blood flow and total hemoglobin concentration decreased at treatment conclusion in each quadrant relative to their respective baseline values. A slight decrease in blood oxygen saturation was also observed.

All three patients showed quantitatively similar hemodynamic responses to PDT. To quantify the dynamic responses, hemodynamic variables before and after PDT were averaged over three patients. Table 1 lists the relative percent decrease after PDT compared to the pre-PDT value in each of the three patients. The mean value and standard error are reported. Average blood flow after PDT decreased ~50% (51.8 ± 7.7%) compared to its baseline, and the total hemoglobin concentration decreased ~15% (14.2 ± 6.2%). The decrease in blood flow was significant (P = 0.02). Conversely, average blood oxygen saturation was essentially constant during PDT (2.9 ± 2.8%).

Table 1. *Relative* hemodynamic changes in human prostate (post-PDT *versus* pre-PDT) in each of three patients (n = 3)

Patient #	# of treatment quadrants	rBF (%)	rTHC (%)	$rStO_2$ (%)
13	3	53.9	13.5	1.5
15	4	37.5	3.8	2.2
17	4	64.0	25.3	8.2
Mean ± SE		51.8 ± 7.7*	14.2 ± 6.2	2.9 ± 2.8

*Significant difference from baseline ($P < 0.05$).

DISCUSSION

Pre-clinical studies have demonstrated that real-time monitoring of PDT hemodynamic responses provides valuable information for prediction/evaluation of treatment efficacy (6,14,23,28). Based on these real-time PDT responses, physicians can potentially adjust treatment conditions (e.g., light dose or illumination intensity) to improve treatment efficacy. However, monitoring hemodynamic responses *during* PDT has proven difficult due to interference between measurement and treatment. For example, PDT studies of murine tumors had to employ a non-contact probe to avoid occlusion of treatment light (23). Translation of these measurements to clinical prostate trials required a substantial modification of the probe-tissue interface. Although several noninvasive optical probes have been made to enable *in vivo* clinical measurements during endoscopic procedures in hollow organs such as the esophagus (15,39), none of them are thin enough to be placed into the 18-gauge catheter (diameter < 1 mm) used for the interstitial prostate PDT. The thin fiber-optic probe developed in this study enabled real-time measurements *during* PDT with minor disturbance of treatment light distribution and negligible patient trauma. The side-illuminating optical fibers of the probe enabled multi-distance source-detector measurements that are essential for accurate tissue spectroscopy. Ultimately, the application of this probe is not limited to prostate PDT. Through endoscopy the probe can be placed on the surface of tumors in organs such as the esophagus and rectum. The method is also suited to application in combination with other treatment modalities, such as radiation therapy.

Photodynamic therapy requires oxygen to cause tumor damage, yet therapy itself can deplete (40) or enhance (41) tumor oxygenation. PDT studies of murine tumors, for example, found that animals experiencing rapid declines in blood flow during PDT showed poor treatment response (23). This finding is consistent with the hypothesis that treatment efficacy is a function of tumor oxygenation during PDT, and under oxygen-limiting conditions, such as rapidly declining blood flow, treatment efficacy can be abrogated. Although tumor oxygenation can be influenced by blood flow, these parameters are not always coupled (41). Simultaneous measurement of both quantities provides deeper insight into tissue physiology. This goal has been achieved in this study.

In this preliminary study of three patients we have found that total hemoglobin concentration (THC) and blood flow decreased during PDT (see Table 1). Together, the observed significant decrease in blood flow (~50%, P = 0.02) and the concurrent decrease in THC (~15%) are consistent with the notion of PDT-induced vascular damage. A slight decrease (~3%) in tumor blood oxygen saturation (StO_2) after PDT was also observed, consistent with observations in the same population measured by a broadband absorption spectroscopy (32).

While it is certainly impossible to draw definite conclusions from measurements of only three patients, the observed differences in tumor blood flow and blood oxygenation responses during PDT can, in principle, be used to choose among tissue oxygen consumption models and therefore emphasize the potential clinical value for simultaneous monitoring of both parameters. For example, the absence of substantial changes in StO_2 during prostate PDT with MLu suggests, among other things, that oxygen consumption may be balanced by another effect. In animal studies Pogue *et al*. (41) observed the tumor partial pressure of oxygen (pO_2) to rise immediately after treatment, and concluded that if oxygen consumption is decreased in the presence of unhindered blood flow tissue, then pO_2 should rise. In the present context, a balance of decreased blood flow and increased cell kill could permit maintenance of StO_2 values. A detailed understanding of these phenomena, however, can only be achieved with more extensive studies, in terms of patient numbers and including studies over a range of light and photosensitizer dose and type.

CONCLUSIONS

We have demonstrated the utility of diffuse correlation spectroscopy (DCS) for monitoring PDT-created blood flow changes, and we have introduced the first clinical use of all-optical methods for measurement of multiple hemodynamic parameters during cancer therapy of the human prostate. These hemodynamic parameters include relative blood flow, tissue blood oxygen saturation and total hemoglobin concentration. In the three patients studied, MLu-mediated PDT was found to decrease tumor blood flow and total hemoglobin concentration. Tumor blood oxygen saturation, however, varied only slightly. The observed differences in response of tumor blood flow and blood oxygenation during PDT further emphasizes the importance of simultaneous monitoring of both parameters.

Acknowledgements—This work is supported in part by grants from Department of Defense (DOD), W81XWH-04-1-0006, and National Institute of Health (NIH), PO1 CA87971-01, R21 CA88064 and 1-R01-HL-077699-01. We thank A. Dimofte and C. Rodriguez for excellent technical assistance.

REFERENCES

1. Dougherty, T. J., C. J. Gomer, B. W. Henderson, G. Jori, D. Kessel, M. Korbelik, J. Moan and Q. Peng (1998) Photodynamic therapy. *J. Natl. Cancer Inst.* **90**, 889–905.
2. Wilson, B. C. (2002) Photodynamic therapy for cancer: Principles. *Can. J. Gastroenterol.* **16**, 393–396.
3. Tromberg, B. J., S. Kimel, A. Orenstein, S. J. Barker, J. Hyatt, J. S. Nelson, W. G. Roberts and M. W. Berns (1990) Tumor oxygen tension during photodynamic therapy. *J. Photochem. Photobiol. B.* **5**, 121–126.
4. Pogue, B. W., R. D. Braun, J. L. Lanzen, C. Erickson and M. W. Dewhirst (2001) Analysis of the heterogeneity of pO2 dynamics during photodynamic therapy with verteporfin. *Photochem. Photobiol.* **74**, 700–706.
5. Sitnik, T. M., J. A. Hampton and B. W. Henderson (1998) Reduction of tumour oxygenation during and after photodynamic therapy in vivo: Effects of fluence rate. *Br. J. Cancer* **77**, 1386–1394.
6. Foster, T. H., R. S. Murant, R. G. Bryant, R. S. Knox, S. L. Gibson and R. Hilf (1991) Oxygen consumption and diffusion effects in photodynamic therapy. *Radiat. Res.* **126**, 296–303.
7. Gross, S., A. Gilead, A. Scherz, M. Neeman and Y. Salomon (2003) Monitoring photodynamic therapy of solid tumors online by BOLD-contrast MRI. *Nat. Med.* **9**, 1327–1331.
8. Wang, L., G. Cull and G. A. Cioffi (2001) Depth of penetration of scanning laser Doppler flowmetry in the primate optic nerve. *Arch. Ophthalmol.* **119**, 1810–1814.
9. Chang, H. Y., C. R. Chen and S. N. Hussain (1995) Diaphragmatic microcirculation measured by laser-Doppler flowmetry in the rat. *J. Appl. Physiol.* **78**, 1225–1233.
10. Tang, S. J., M. L. Gordon, V. X. Yang, M. E. Faughnan, M. Cirocco, B. Qi, E. S. Yue, G. Gardiner, G. B. Haber, G. Kandel, P. Kortan, A. Vitkin, B. C. Wilson and N. E. Marcon (2003) In vivo Doppler optical coherence tomography of mucocutaneous telangiectases in hereditary hemorrhagic telangiectasia. *Gastrointest. Endosc.* **58**, 591–598.
11. Chen, Z., T. E. Milner, X. Wang, S. Srinivas and J. S. Nelson (1998) Optical Doppler tomography: Imaging in vivo blood flow dynamics following pharmacological intervention and photodynamic therapy. *Photochem. Photobiol.* **67**, 56–60.
12. Gee, M. S., H. M. Saunders, J. C. Lee, J. F. Sanzo, W. T. Jenkins, S. M. Evans, G. Trinchieri, C. M. Sehgal, M. D. Feldman and W. M. Lee (2001) Doppler ultrasound imaging detects changes in tumor perfusion during antivascular therapy associated with vascular anatomic alterations. *Cancer Res.* **61**, 2974–2982.
13. Durduran, T., R. Choe, J. P. Culver, L. Zubkov, M. J. Holboke, J. Giammarco, B. Chance and A. G. Yodh (2002) Bulk optical properties of healthy female breast tissue. *Phys. Med. Biol* **47**, 2847–2861.
14. Pham, T. H., R. Hornung, M. W. Berns, Y. Tadir and B. J. Tromberg (2001) Monitoring tumor response during photodynamic therapy using near-infrared photon-migration spectroscopy. *Photochem. Photobiol.* **73**, 669–677.
15. Bays, R., G. Wagnieres, D. Robert, D. Braichotte, J. Savary, P. Monnier and H. van den Bergh (1996) Clinical determination of tissue optical properties by endoscopic spatially resolved reflectometry. *Appl. Opt.* **35**, 1756–1766.
16. Boas, D. A., L. E. Campbell and A. G. Yodh (1995) Scattering and imaging with diffusing temporal field correlations. *Phys. Rev. Letters* **75**, 1855–1858.
17. Culver, J. P., T. Durduran, D. Furuya, C. Cheung, J. H. Greenberg and A. G. Yodh (2003) Diffuse of optical tomography cerebral blood flow, oxygenation and metabolism in rat during focal ischemia. *J. Cerebral Blood Flow & Met.* **23**, 911–924.
18. Cheung, C., J. P. Culver, K. Takahashi, J. H. Greenberg and A. G. Yodh (2001) In vivo cerebrovascular measurement combining diffuse near-infrared absorption and correlation spectroscopies. *Phys. Med. Biol.* **46**, 2053–2065.
19. Durduran, T., G. Yu, M. G. Burnett, J. A. Detre, J. H. Greenberg, J. Wang, C. Zhou and A. G. Yodh (2004) Diffuse optical measurement of blood flow, blood oxygenation, and metabolism in a human brain during sensorimotor cortex activation. *Opt. Lett.* **29**, 1766–1768.
20. Zhou, C., G. Q. Yu, D. Furuya, J. H. Greenberg, A. G. Yodh and T. Durduran (2006) Diffuse optical correlation tomography of cerebral blood flow during cortical spreading depression in rat brain. *Opt. Exp.* **14**, 1125–1144.
21. Menon, C., G. M. Polin, I. Prabakaran, A. Hsi, C. Cheung, J. P. Culver, J. F. Pingpank, C. S. Sehgal, A. G. Yodh, D. G. Buerk and D. L. Fraker (2003) An integrated approach to measuring tumor oxygen status using human melanoma xenografts as a model. *Cancer Res.* **63**, 7232–7240.
22. Durduran, T., R. Choe, G. Yu, C. Zhou, J. C. Tchou, B. J. Czerniecki and A. G. Yodh (2005) Diffuse optical measurement of blood flow in breast tumors. *Opt. Lett.* **30**, 2915–2917.
23. Yu, G., T. Durduran, C. Zhou, H. W. Wang, M. E. Putt, H. M. Saunders, C. M. Sehgal, E. Glatstein, A. G. Yodh and T. M. Busch (2005) Noninvasive monitoring of murine tumor blood flow during and after photodynamic therapy provides early assessment of therapeutic efficacy. *Clin. Cancer Res.* **11**, 3543–3552.
24. Yu, G., T. Durduran, G. Lech, C. Zhou, B. Chance, E. R. Mohler and A. G. Yodh (2005) Time-dependent blood flow and oxygenation in human skeletal muscles measured with noninvasive near-infrared diffuse optical spectroscopies. *J. Biomed. Opt.* **10**, 024027.
25. Yu, G., T. Durduran, D. Furuya, J. H. Greenberg and A. G. Yodh (2003) Frequency-domain multiplexing system for in vivo diffuse light measurements of rapid cerebral hemodynamics. *Appl. Opt.* **42**, 2931–2939.
26. Choe, R., T. Durduran, G. Yu, M. J. Nijland, B. Chance, A. G. Yodh and N. Ramanujam (2003) Transabdominal near infrared oximetry of

hypoxic stress in fetal sheep brain in utero. *Proc. Natl. Acad. Sci.* **100**, 12950–12954.
27. Choe, R. (2005) Diffuse Optical Tomography and Spectroscopy of Breast Cancer and Fetal Brain, Ph.D. dissertation, University of Pennsylvania, Philadelphia.
28. Wang, H. W., M. E. Putt, M. J. Emanuele, D. B. Shin, E. Glatstein, A. G. Yodh and T. M. Busch (2004) Treatment-induced changes in tumor oxygenation predict photodynamic therapy outcome. *Cancer Res.* **64**, 7553–7561.
29. Jemal, A., T. Murray, A. Samuels, A. Ghafoor, E. Ward and M. J. Thun (2003) Cancer statistics 2003. *CA Cancer J. Clin.* **53**, 5–26.
30. Mody, T. D., L. Fu and J. L. Sessler (2001) *Texaphyrins: Synthesis and Development of a Novel Class of Therapeutic Agents*. Karlin KDE, pp. 551–598. John Wiley & Sons, Ltd., Chichester.
31. Young, S. W., K. W. Woodburn, M. Wright, T. D. Mody, Q. Fan, J. L. Sessler, W. C. Dow and R. A. Miller (1996) Lutetium texaphyrin (PCI-0123): A near-infrared, water-soluble photosensitizer. *Photochem. Photobiol.* **63**, 892–897.
32. Zhu, T. C., A. Dimofte, J. C. Finlay, D. Stripp, T. Busch, J. Miles, R. Whittington, S. B. Malkowicz, Z. Tochner, E. Glatstein and S. M. Hahn (2005) Optical properties of human prostate at 732 nm measured in mediated photodynamic therapy. *Photochem. Photobiol.* **81**, 96–105.
33. Zhu, T. C., J. C. Finlay and S. M. Hahn (2005) Determination of the distribution of light, optical properties, drug concentration, and tissue oxygenation in-vivo in human prostate during motexafin lutetium-mediated photodynamic therapy. *J. Photochem. Photobiol. B.* **79**, 231–241.
34. Boas, D. A. (1996) Diffuse Photon Probes of Structural and Dynamical Properties of Turbid Media: Theory and Biomedical Applications. Ph.D. dissertation, University of Pennsylvania, Philadelphia.
35. Pine, D. J., D. A. Weitz, P. M. Chaikin and Herbolzheimer (1988) Diffusing-wave spectroscopy. *Phys. Rev. Lett.* **60**, 1134–1137.
36. Maret, G. and P. E. Wolf (1987) Multiple light scattering from disordered media. The effect of Brownian motion of scatterers. *Z. Phys. B* **65**, 409–413.
37. Boas, D. A. and A. G. Yodh (1997) Spatially varying dynamical properties of turbid media probed with diffusing temporal light correlation. *Journal of the Optical Society of America a-Optics Image Science and Vision* **14**, 192–215.
38. Weersink, R. A., A. Bogaards, M. Gertner, S. R. Davidson, K. Zhang, G. Netchev, J. Trachtenberg and B. C. Wilson (2005) Techniques for delivery and monitoring of TOOKAD (WST09)-mediated photodynamic therapy of the prostate: Clinical experience and practicalities. *J. Photochem. Photobiol. B.* **79**, 211–222.
39. Yang, V. X. D., M. Gordon, S. J. Tang, N. Marcon, G. Gardiner, B. Qi, S. Bisland, E. Seng-Yue, S. Lo, J. Pekar, B. C. Wilson and I. Vitkin (2003) High speed, wide velocity dynamic range Doppler optical coherence tomography (Part III): In vivo endoscopic imaging of blood flow in the rat and human gastrointestinal tracts. *Opt. Exp.* **11**, 2416–2424.
40. Busch, T. M., S. M. Hahn, S. M. Evans and C. J. Koch (2000) Depletion of tumor oxygenation during photodynamic therapy: Detection by the hypoxia marker EF3 [2-(2-nitroimidazol-1[H]-yl)-N-(3,3,3-trifluoropropyl)acetamide]. *Cancer Res.* **60**, 2636–2642.
41. Pogue, B. W., J. A. O'Hara, E. Demidenko, C. M. Wilmot, I. A. Goodwin, B. Chen, H. M. Swartz and T. Hasan (2003) Photodynamic therapy with verteporfin in the radiation-induced fibrosarcoma-1 tumor causes enhanced radiation sensitivity. *Cancer Res.* **63**, 1025–1033.